JOURNAL OF GEOPHYSICAL RESEARCH VOL. 69, NO. 13 JULY 1, 1964

Satellite Observations of the Geomagnetic Field during Magnetic Storms[1]

E. J. SMITH[2]

Space Technology Laboratories, Redondo Beach, California

C. P. SONETT AND J. W. DUNGEY[3]

Space Sciences Division, Ames Research Center
National Aeronautics and Space Administration
Moffett Field, California

Abstract. Explorer 6 satellite data and surface magnetograms are used to study the gradual and sudden commencement geomagnetic storms of August 16–18, 1959. Analysis of these data provides the following conclusions: (1) The geomagnetic field was strongly perturbed but retained its essentially dipolar character out to geocentric distances of 8 earth radii. (2) A long-period variation in the distant field coincided with D_{st} at the surface. The magnitude of the main-phase decrease at $\sim 4R_E$ was ~ 2.5 times larger than at the surface. Variations in the field direction at $\sim 7R_E$ correlate with half-day variations in (*a*) the horizontal component at the surface and (*b*) the 3-hour K index. (3) Large irregular field fluctuations with periods exceeding one minute were characteristic of the storm period. (4) The large-scale storm field was qualitatively similar to the disturbance field observed previously on nonstorm days. The disturbance field appeared to evolve from quiet to disturbed conditions and then to gradually recover.

INTRODUCTION

Simultaneous measurements of the geomagnetic field at the surface and in the magnetosphere are essential to a better understanding of magnetic storms, since the solar effects responsible for storms can be strongly modified by a complicated interaction with the earth's outer atmosphere. Space probes Pioneer 1 and Lunik 2 [*Sonett, Judge, Sims, and Kelso,* 1960; *Krassovsky,* 1960] traversed the distant geomagnetic field during nonstorm intervals. Pioneer 5 and Lunik 1 were launched during the recovery phases of storms [*Coleman et al.,* 1960], and Vanguard 3 (apogee ~10,000 km) measured the field above the ionosphere during an interval which included several moderate magnetic storms [*Heppner et al.,* 1960]. Explorer 6 made the first repetitive measurements of the earth's field, between 4 and $8R_E$ (earth radii), during a magnetic storm.

The satellite magnetic field data obtained by Explorer 6 at geocentric distances between 4 and $8R_E$ during a severe magnetic storm are used here to study the gross characteristics of the large-scale storm field surrounding the earth. The physical origin of the storm field is investigated, as is the possible existence of a main phase ring current. Long-period variations in the distant field are also compared with variations in the intensity of the outer radiation zone during the storm. Some of the data discussed here have been published previously in a preliminary report [*Smith and Sonett,* 1962].

BACKGROUND

Instrumentation. The detecting element of the magnetometer, a solenoid wound on a high permeability core, was attached to the shell of the spin-stabilized spacecraft which rotated 2.7 times per second. In an ambient stationary magnetic field, a sinusoidal voltage was generated with a frequency equal to the spin rate and an amplitude proportional to $B_\perp$, the component of the magnetic field perpendicular to the spacecraft spin axis (Figure 1). The electronics consisted of an amplifier having a passband centered at the spin frequency. A quasilogarithmic amplifier

[1] Parts of this paper were presented at the International Conference on Cosmic Rays and the Earth Storm, Kyoto, September 1961 [*Smith and Sonett,* 1962].

[2] Permanent address: Space Sciences Division, Jet Propulsion Laboratory, Pasadena, California.

[3] Permanent address: Department of Physics, Imperial College, London.

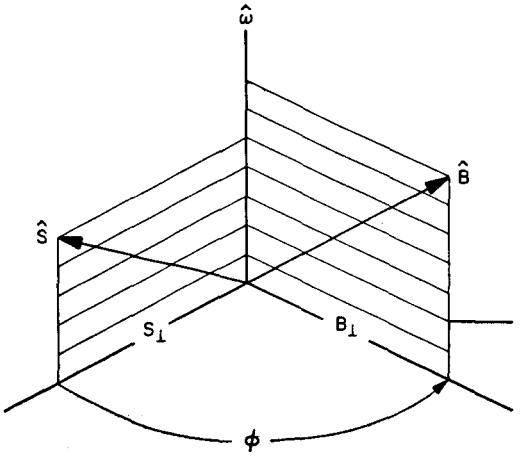

Fig. 1. Spacecraft coordinate system. This figure shows the essential features of the experiment geometry. $\hat{\omega}$ is the rotation axis of the spin-stabilized spacecraft. The equatorial plane of the spacecraft is perpendicular to $\hat{\omega}$. $\hat{S}$ is a unit vector directed toward the sun, and B is the magnetic field vector. The projections of $\hat{S}$ and B onto the equatorial plane are $S_\perp$ and $B_\perp$, respectively, which define the angle ϕ. The Explorer 6 magnetometer measured $B_\perp$ and ϕ directly.

gain, achieved by using automatic gain control, extended the dynamic range of the magnetometer to 3 orders of magnitude so that fields could be measured over an extended range of altitudes.

The magnetometer coil constant, the numerical relation between field strength and the induced voltage, was determined by comparing the voltages generated when the search coil and a standard air-core coil were simultaneously rotated in the earth's field in a region where gradients were small. Sinusoidal input voltages were used to obtain steady-state electronic calibration. (The transient response of the magnetometer is not pertinent to this paper and will be discussed elsewhere.) In a given field, the output signal amplitude depended on the spin rate of the spacecraft and was only slightly dependent on the temperature of the electronics which was checked by means of several temperature sensors inside the spacecraft. The satellite spin rate was computed on the ground from the number of cycles of the telemetered sinusoid that occurred in a given time period. Further details about the equipment and its calibration are reported elsewhere [*Judge et al.*, 1960].

Early recognition of the importance of directional data [*Sonett et al.*, 1959] led to the inclusion of a photodiode sun scanner and phase comparator. This instrument provided a phase reference, based on the solar direction, and determined, in flight, the directional variations in $B_\perp$. The merit of including this type of instrument has been supported by subsequent events, and sun scanners are now virtually standard equipment on spinning spacecraft.

The phase comparator measured the angle φ between $B_\perp$ and $S_\perp$, where $S_\perp$ is the projection into the spacecraft equatorial plane of a unit vector pointing from the spacecraft in the direction of the sun (Figure 1). Hereafter, φ is called the *phase angle*. It is the magnetic declination in spacecraft coordinates referred to the spacecraft-sun direction, and it depends on the orientation of the spacecraft spin axis.

The phase comparator input signals were the search coil sinusoid and a sequence of pulses generated by a photodiode when illuminated by solar radiation once per spacecraft revolution (Figure 2). The photodiode pulse and a pulse coincident with the zero-voltage crossing of the search coil sinusoid operated Schmidt triggers that controlled the state of a flip-flop. The output, obtained by integration of the flip-flop output signal, was a dc voltage proportional to the time delay between the two pulses. Except for very small fields, the phase comparator output was independent of the magnitude of the search coil sinusoid, and the measurement of φ was independent of $B_\perp$.

The search coil and phase comparator analog voltages each modulated a subcarrier oscillator. The resulting FM signals, which were transmitted continuously, were received at one or more STL ground stations (England, Florida, Hawaii, and Singapore) approximately 18 hours per day. The search coil sinusoid was also converted to a slowly varying dc voltage by a peak detector and filter and was digitized inside the spacecraft along with the phase comparator output. Transmissions of binary-coded digital data, which were used to test the telemetry system subsequently flown on Pioneers, were commanded from the ground at irregular intervals. The digital data were used primarily to check the quality and accuracy of the telemetered analog data.

Orbit parameters. After Explorer 6 was launched in August 1959, much time and effort was expended in refining the ephemeris because

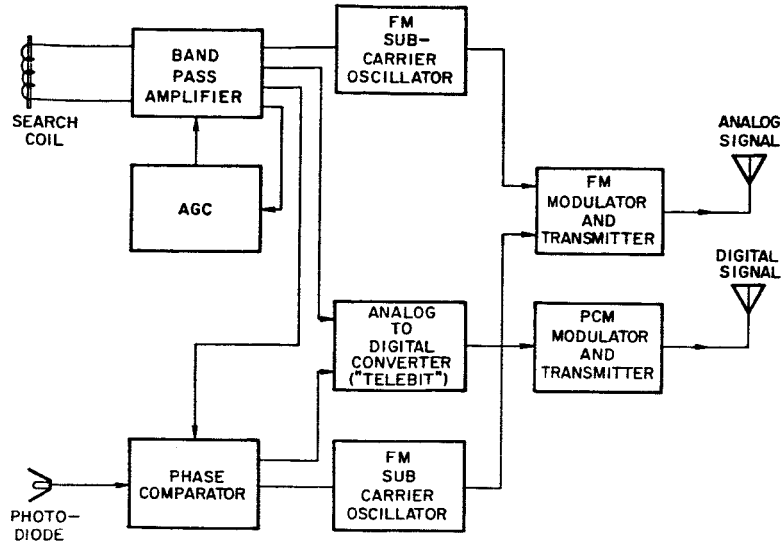

Fig. 2. Block diagram of the search coil magnetometer. The experiment sensors are the search coil and a sun-sensing photodiode. The amplifier bandpass was centered at the spacecraft spin frequency and automatic gain control extended the dynamic range of the amplifier. The phase comparator measured the time delay between zero-voltage crossings of the search coil sinusoid (corresponding to the instant when the directions of $B_\perp$ and the coil axis coincided) and pulses generated when the sun was within the narrow field of view of the photodiode. Two independent data processing systems were employed. Analog voltages were telemetered continuously as frequency-modulated signals. The analog voltages were also converted to binary numbers on the spacecraft and transmitted on ground command.

of perigee drag fluctuations and solar-lunar perturbations, a poorly understood subject in 1959. With the establishment of an accurate orbit and a precise spin axis orientation, the more subtle effects in the data, such as the properties of the disturbance field near the geomagnetic equator, were made accessible.

The Explorer 6 orbit (apogee 48,000 km, perigee 6740 km) was highly eccentric. The orbital plane was inclined 47° to the geographic equator and apogee was at geographic latitude −20°. The spacecraft crossed the equatorial plane at geocentric altitudes of 7200 and 30,000 km. Figure 3 shows a projection of the orbit onto the surface of the earth during August 16–17.

The satellite was launched from Atlantic Missile Range at 1345 GMT on August 7, 1959. Since perigee occurred at about 0900 hours local time, apogee was on the opposite side of the earth at 2100 hours local time. On August 7, the projection onto the geographic equatorial plane of the semimajor axis of the orbit made an angle of ~135° with respect to the earth-sun direction. This angle decreased by approximately 1° per day. The right ascension and declination of the spin axis were 217° and 23°, respectively.

The orbital period, 12¾ hours, had an important effect on the instantaneous location of the spacecraft in geomagnetic coordinates. Because the earth's magnetic pole is inclined 11½° with respect to the rotation axis, the geomagnetic latitude of a given orbital position underwent a semidiurnal variation as large as 23°. However, the geomagnetic latitude of the spacecraft was nearly the same before and after two complete rotations around the earth (~25½ hours). This prompted us to divide the data obtained on odd-numbered and even-numbered passes into two separate groups in order to isolate temporal changes in the geomagnetic field more clearly.

Magnetic conditions at the earth's surface. August 12, 13, and 14 were among the five quietest days in August [*Lincoln*, 1960] (Figure 4). On August 15, a gradual commencement storm was reported at some stations. At approximately 0400 on August 16, a sudden commencement storm began and continued until the end

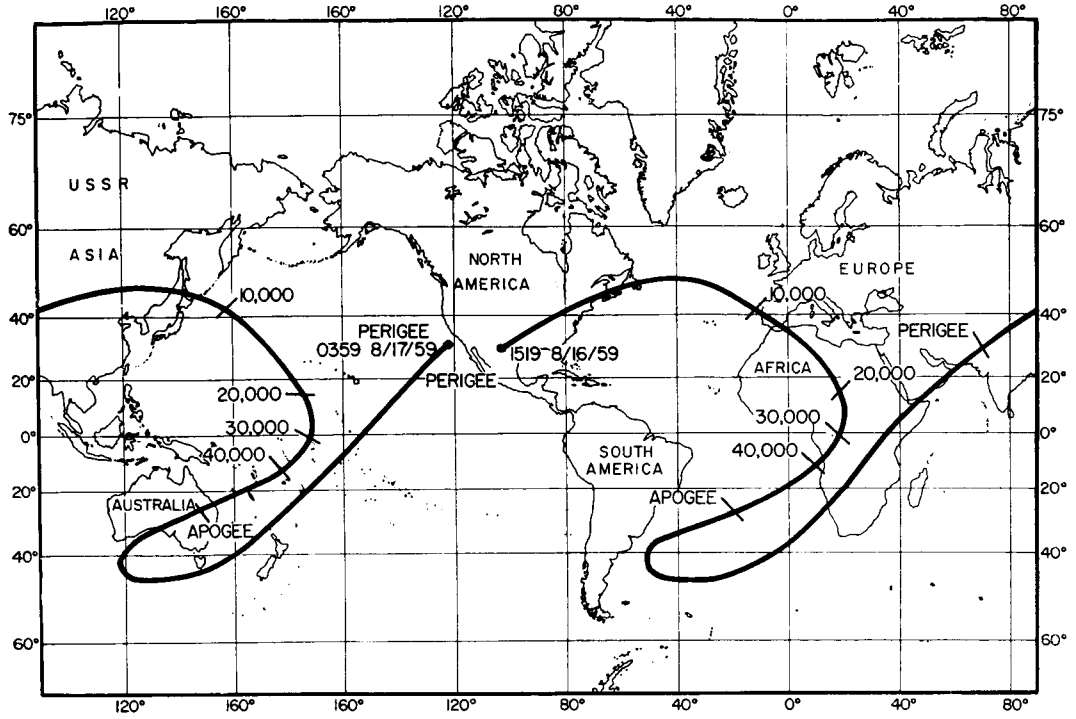

Fig. 3. Projection of the Explorer 6 trajectory on to the earth. The geographic position of the spacecraft is shown at radial distances separated by 10,000 km and at apogee. The positions shown are for the 18th orbit on August 16–17.

of August 17 or the beginning of August 18. This storm was classed as severe (corresponding to a K index of 8 or 9). Huancayo reported a moderate, gradual commencement storm which began at 0635 on August 18 and ended at 2000 hours the same day. A moderately severe sudden commencement storm began on August 20 at 0412. There is no general agreement as to when this storm ended. (Some stations estimated that it ended on August 20, but others recorded disturbed conditions until August 24.) August 27 and 28 were the two quietest days of the month. A moderately severe ($K = 6, 7$) sudden commencement storm began on September 3 at 2159 and continued until September 5 or 6. The discussion which follows is concerned primarily with the severe magnetic storm of August 16.

Review of the Explorer 6 data obtained on nonstorm days. In the preliminary analysis of the data, the magnitude $B_\perp$ and direction φ of the observed field were compared with the magnitude and direction of the extrapolated geomagnetic field [*Sonett, Smith, Judge, and Coleman*, 1960; *Sonett, Smith, and Sims*, 1960; *Smith et al.*, 1960]. An 8 coefficient spherical-harmonic expansion of the surface field [*Vestine*, 1959] was used to extrapolate the geomagnetic surface field to the satellite position, where it was resolved into spacecraft coordinates for comparison with the measured field. This computed field is labeled $G_\perp$ and has spacecraft declination φ_G.

Discrepancies between $B_\perp$, the measured component, and $G_\perp$, the extrapolated one, were observed throughout most of the trajectory. Below $5R_E$, $B_\perp$ tends to exhibit the same altitude dependence as $G_\perp$ but to have a somewhat larger magnitude. Beyond approximately $5R_E$, there was a marked disparity between $B_\perp$, $G_\perp$, and their spacecraft declinations, φ and φ_G.

An important consequence of the AGC loop is that the relative and absolute accuracy of measurement increased with increasing altitude. For example, a change of 1 per cent in the output voltage corresponded to 300 γ in a 5000 γ

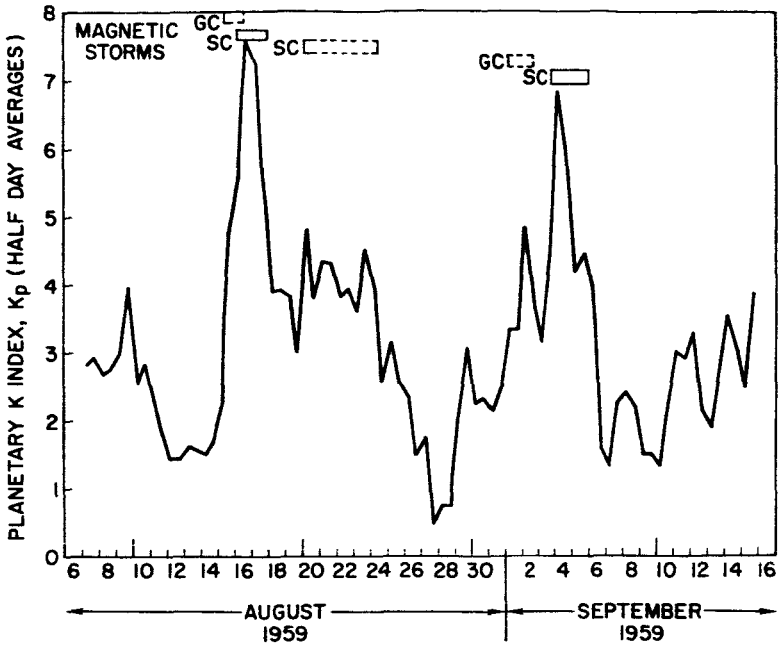

Fig. 4. Geomagnetic activity during the Explorer 6 epoch. The planetary K index, K_p, is shown for August 7 to September 15, 1959. Half-day averages are plotted because the orbital period of the Explorer 6 was approximately 12¾ hours. The major storms are indicated at the top of the figure where GC and SC stand for gradual and sudden commencement storms, respectively. The lengths of the rectangles indicate the duration of the storm and are dashed where uncertainties exist.

field (approximate altitude, 12,000 km), and to only 3 γ in a 100 γ field (approximate altitude, 38,000 km). The differences between $B_\perp$ and $G_\perp$ beyond $5R_E$ corresponded to large fractional changes (15 to 20 per cent) in the magnetometer output signal. The experimental results suggested that the extraterrestrial field was essentially dipolar out to $5R_E$, deviating progressively at greater altitudes. (The deviation between $G_\perp$ and $B_\perp$ depends strongly on the direction of $B_\perp$, as well as on its magnitude.) In a preliminary survey of data obtained throughout a 6-week interval, large-scale perturbations in $B_\perp$ and φ were always noted, although their shapes varied from day to day and were strongly dependent on the geometry of the experiment.

A perturbation field based on an equatorial current with a finite, circular cross section and constant current density was used to explore possible causes of the observed differences. The field due to the current was computed at points on the trajectory and added vectorially to the geomagnetic field; a coordinate transformation was then performed to obtain theoretical values of $B_\perp$ and φ. Reasonable agreement between the data and the model calculations was obtained for a westward current of $5 \cdot 10^6$ amperes centered at $10R_E$ [*Smith et al.*, 1960].

Perturbations in the distant geomagnetic field were also subsequently observed by Pioneer 5 on the sunward side of the earth. When the same mathematical model was applied to the Pioneer 5 magnetometer data obtained inside the geomagnetic field, reasonable agreement was again obtained between the calculated and observed $B_\perp$ for a westward current of $5 \cdot 10^6$ amperes centered at $8R_E$ and extending from 5 to $11R_E$.

These model calculations, employing an ad hoc current, were justifiably criticized because they ignored an important feature of currents associated with trapped particles. The diamagnetic character of the trapped particles should lead to a maximum reduction of the geomagnetic field at the peak of the particle kinetic energy distribution. *Akasofu and Chapman* [1961] compared the Explorer 6 data for August 9 with a computed field based on a model radiation zone. Their results place the particles at $\sim 6R_E$ and suggest

the total current was $\sim 2 \cdot 10^6$ amperes. Similarly, *Apel et al.* [1962] derived a distribution of trapped particles corresponding to the Pioneer 5 magnetometer data and found it to be centered at $\sim 6R_E$. Although both these calculations employed ideal rather than observed particle distributions and did not take into account geometrical effects associated with the data, such as the geomagnetic latitude and spin axis orientation of the spacecraft, they undoubtedly lead to a more realistic estimate of where the particles causing the Explorer 6 and Pioneer 5 field deformations were located than our preliminary model calculations. For example, compare the vector disturbance field computed by *Akasofu et al.* [1961, Figure 1] with the vector field derived from the Explorer 6 measurements [*Smith*, 1962, Figure 1].

It should be noted that the model calculations were applied to data obtained under disturbed magnetic conditions. The Pioneer 5 data were acquired during the recovery of a moderate magnetic storm. The Explorer 6 data obtained on August 9 were initially regarded as nonstorm data because a preliminary classification did not list August 9 as a disturbed day. However, as Figure 4 shows, the K_p index reached a value of 4 during the period in which the data were obtained. All periods in which K_p exceeded 4 included storms.

The Experimental Data

The data in Figure 5 were obtained on three successive days during the severe SC storm which began on August 16.

The storm data show the same qualitative features as the data obtained on nonstorm days (e.g., see Figure 1 in *Sonett, Smith, Judge, and Coleman*, [1960]). For example, the fine structure appearing in Figure 5, a variation of several hundred gammas that occurred at 30,000 km on August 17, may be the result of either spatial or temporal variations and is a subject of special interest investigated separately in connection with bay-like, polar storm variations [*Smith and Judge*, 1961].

In interpreting the data, we assumed that the field was perpendicular to the equatorial plane on the geomagnetic equator for both quiet and storm-time fields. Therefore, the scalar field measured at the equator completely specified the resultant field. For nonequatorial points of observation, variations in $B_\perp$ were caused by a change in the direction as well as in magnitude of the field. Thus, treating the equatorial measurements separately will simplify the interpretation of the experimental data. The next section describes the time dependence of the field magnitude near the geomagnetic equatorial plane. This is followed by a discussion of field direction at points of observation below the

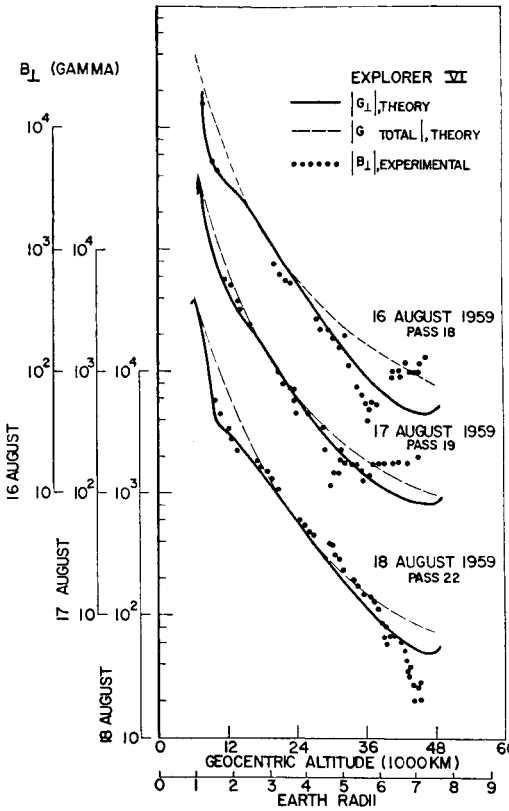

Fig. 5. Explorer 6 field magnitude data for the magnetic storm of August 16–18. $B_\perp$ is shown as a function of geocentric distance for 3 orbits on August 16, 17, and 18. Values of the total geomagnetic field G and the component perpendicular to the satellite spin axis direction $G_\perp$ are also shown. $G_\perp$ and G are approximately equal from 3 to $4R_E$ because the Explorer 6 spin axis is nearly orthogonal to the geomagnetic field vector. The differences between $B_\perp$ and $G_\perp$, which appear to be large at geocentric distances of less than 3 earth radii, are exaggerated by the quasi-logarithmic characteristic of the magnetometer amplifier. The deviation between $B_\perp$ and $G_\perp$ at $R > 5R_E$ first noted on nonstorm days is also observed during the storm.

equatorial plane. The centered dipole approximation of the geomagnetic field is used to define the geomagnetic equator.

Variation in the magnitude of the near-equatorial field during the storm. Figure 6*a* shows the time variation of the field magnitude in the outer radiation zone. Each datum was obtained from a measurement of $B_\perp$ at a geocentric distance of approximately 24,000 km or $4R_E$ (the actual radial distance varied between 22,000 and 26,000 km). The corresponding value of the extrapolated geomagnetic field was computed and subtracted from $B_\perp$. The differences ($\Delta B_\perp = B_\perp - G_\perp$) are plotted in Figure 6*a* for approximately the first two weeks of Explorer 6 observations. Since the observed field at 24,000 km tends to exceed the

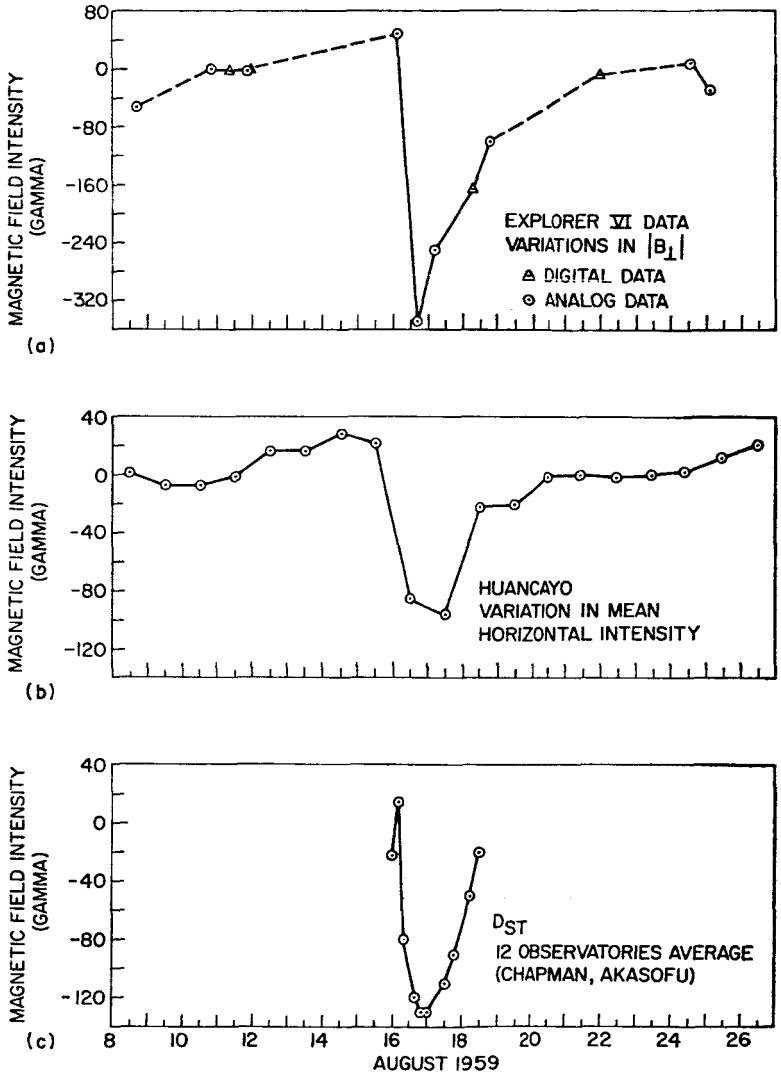

Fig. 6. Time variations of the equatorial disturbance field compared with D_{st} variation at the earth's surface. (*a*) $\Delta B_\perp = B_\perp - G_\perp$ at $\sim 4R_E$ near the geomagnetic equator during the first two weeks of Explorer 6 measurements. The data are normalized so that $\Delta B_\perp = 0$ on August 12 (one of the magnetically quietest days of the month). (*b*) The variation in the horizontal intensity of the surface field at Huancayo, Peru ($\delta_M = -0.6°$). Daily averages are plotted at 1200 GMT. (*c*) The D_{st} curve for the SC storm of August 16; this curve was derived by S. Chapman and S.-I. Akasofu by averaging the storm data from 12 geomagnetic observatories.

extrapolated surface field on magnetically quiet days, a feature of the data that could be caused by a lack of good absolute accuracy at this altitude, the data in Figure 6*a* were adjusted so that $\Delta B_\perp = 0$ on the quietest days of the month (August 11–12) by subtracting the amount by which $B_\perp$ exceeded $G_\perp$ on August 11 from all the differences. The digital data appearing in Figure 6*a*, which were similarly adjusted, provide data for times for which no analog data were available.

Figure 6*b* is the time variation of the horizontal component of the surface field. Each datum, the daily mean value of the horizontal intensity at Huancayo, Peru (geomagnetic latitude δ_M, $-0.6°$), obtained by averaging the hourly mean values over each Greenwich day, has been plotted at 1200 GMT. This procedure produced a reasonable representation of long-period changes in the earth's field. The variation in mean horizontal intensity has also been biased so that $\Delta H = 0$ on August 11–12.

The outstanding feature of the Huancayo data is the superimposed magnetic storms of August 15–20. The storm period was preceded and followed by quiet intervals during which the horizontal component rose to its highest values (August 14–15, 26–28). The effect of the SC storm which began on August 16 is particularly noticeable.

Figure 6*c*, which is a plot of the smoothed D_{st} curve derived by Chapman and Akasofu [*Arnoldy et al.*, 1960], shows the history of the August 16 storm in greater detail. The data are averages of the horizontal component measured at 12 observatories well distributed in latitude and longitude.

The long-period variation of the storm field at the surface coincides with a similar variation at an altitude of ~4 earth radii (24,000 km). A comparison of Figures 6*a*, *b*, and *c* indicates that $B_\perp$ undergoes a main phase decrease and recovery at $\sim 4R_E$ which is essentially coincident with D_{st} at the surface. The magnitude of the main phase decrease is ~140 γ at the surface and ~360 γ at $4R_E$, that is, approximately two and one-half times as large.

Variation in the direction of the field during the storm. Magnitude data ($B_\perp$) are unavailable for parts of the Explorer 6 orbit and for much of the

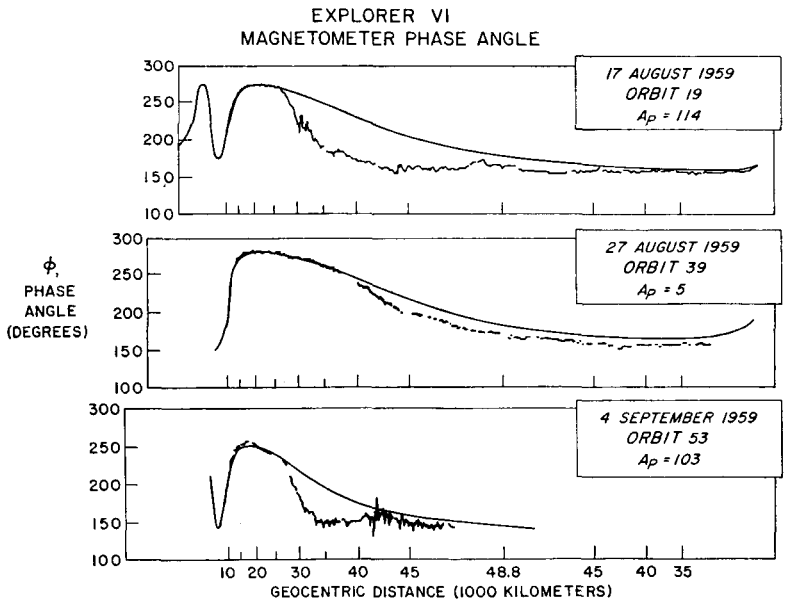

Fig. 7. Phase angle data during storm and nonstorm intervals. The phase angle ϕ is shown as a function of geocentric distance for orbits on August 17 and 27 and September 4. The theoretical angle based on a spherical harmonic expansion of the surface field is also shown. August 17 and September 4 were storm days, and August 27 was the quietest day of the month. The planetary A_p indices are shown for each day. There are substantial changes in the character of the large-scale deviation, $\phi - \phi_0$, between quiet and disturbed periods. In addition, during storm periods irregular small-scale variations in ϕ are typical.

Explorer 6 lifetime. When the satellite was at large radial distances, it was difficult to obtain good quality ground station records because of the relatively broad bandwidth requirements of the sinusoidal output signal and the low power of the radiated telemetry signal, which was significantly below the design goal. Most of the useful magnitude data were acquired by the large radio telescope at Jodrell Bank, England, Conversely, the frequency-modulated signal from the phase comparator varied slowly over the orbit, the signal bandwidth was narrow, and most of the phase data were eventually recovered.

Figure 7 shows the departure of the observed field direction from the direction of the extrapolated geomagnetic field and contrasts the departures on storm days and quiet days. The experimental measurements obtained from the magnetic field aspect indicator (or phase comparator) are shown as a function of altitude for

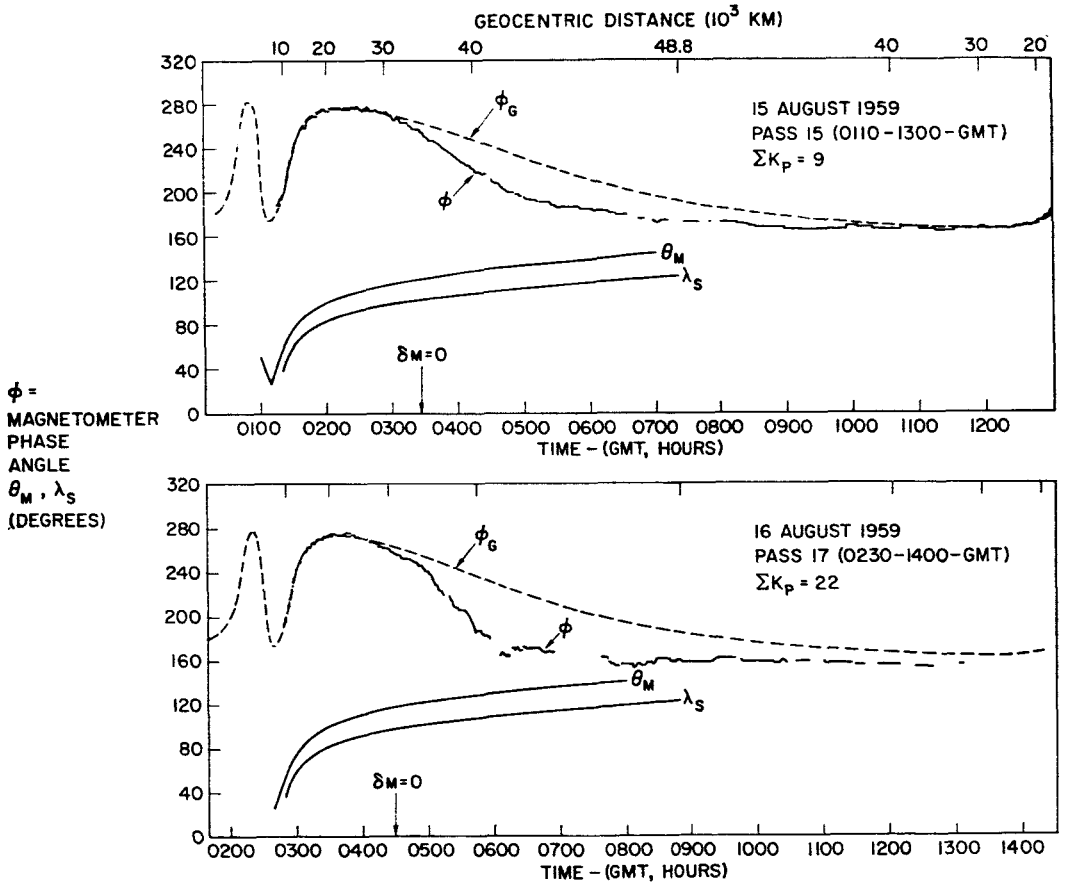

Fig. 8. Phase data obtained during a magnetic storm (odd-numbered passes). The phase angle ϕ is shown as a function of geocentric distance and universal time. The theoretical phase angle for the unperturbed geomagnetic field, ϕ_G, is also shown. θ_M is the angle between the Explorer 6 spin axis and the local magnetic meridian plane (see Figure 13). λ_S is the angle between the projection of the spacecraft radius and the earth-sun direction on to the geographic equatorial plane (see Figure 14). The arrow marked $\delta_M = 0$ indicates where the spacecraft crossed the geomagnetic equator. Data are shown for two orbits, numbers 15 and 17 on August 15 and 16. The odd-numbered passes are presented together because their trajectories are similar in geomagnetic coordinates. ΣK_p is the sum of the planetary K indices during the 12 hours of each orbit. Note the agreement between ϕ and ϕ_G at low geocentric altitudes, which represents a calibration check on the phase comparator data at high altitudes where large deviations from the geomagnetic field direction are observed.

three orbital passes. Also shown are theoretical values of the phase angle for the extrapolated geomagnetic field (φ_G).

At geocentric distances of less than 10,000–15,000 km, $\varphi = \varphi_G$ because of the 'stiffness' of the geomagnetic field near the earth (i.e., a transverse disturbance field of several hundred gamma would not produce an observable change in the direction of the dipole field lines). Fortunately, the same range of angles ($150° < \varphi < 300°$) was observed near the earth and at great distances. Thus the agreement between φ and φ_G near perigee provides a check on the consistency of the aspect indicator calibration.

At large distances from the earth, where Explorer 6 was at southern geomagnetic latitudes, the phase deviation $\Delta\varphi = \varphi - \varphi_G$ was negative. On the geomagnetic equator ($\delta_M = 0$ is indicated in Figures 8 through 11, and the geomagnetic latitude of the spacecraft as it traveled from 20,000 km to apogee is shown in Figure 14), $\Delta\varphi$ was either zero (passes 16, 18, and 20) or slightly negative (orbits 15, 17, 19, 21, and 22).

The extent by which φ differed from φ_G depended, in part, on the trajectory of the Explorer 6 (i.e., the magnetic latitude of the spacecraft at a given altitude). There was also a time variation apparent in Figure 7. Magnetic storms occurred August 17 and September 4, whereas August 27 was one of the quietest days of the month (A_p indices are included in the figure).

On August 27 and 13, $\Delta\varphi$ was smallest when, as Figure 6 indicates, the horizontal intensity at the earth's surface rose to its highest value.

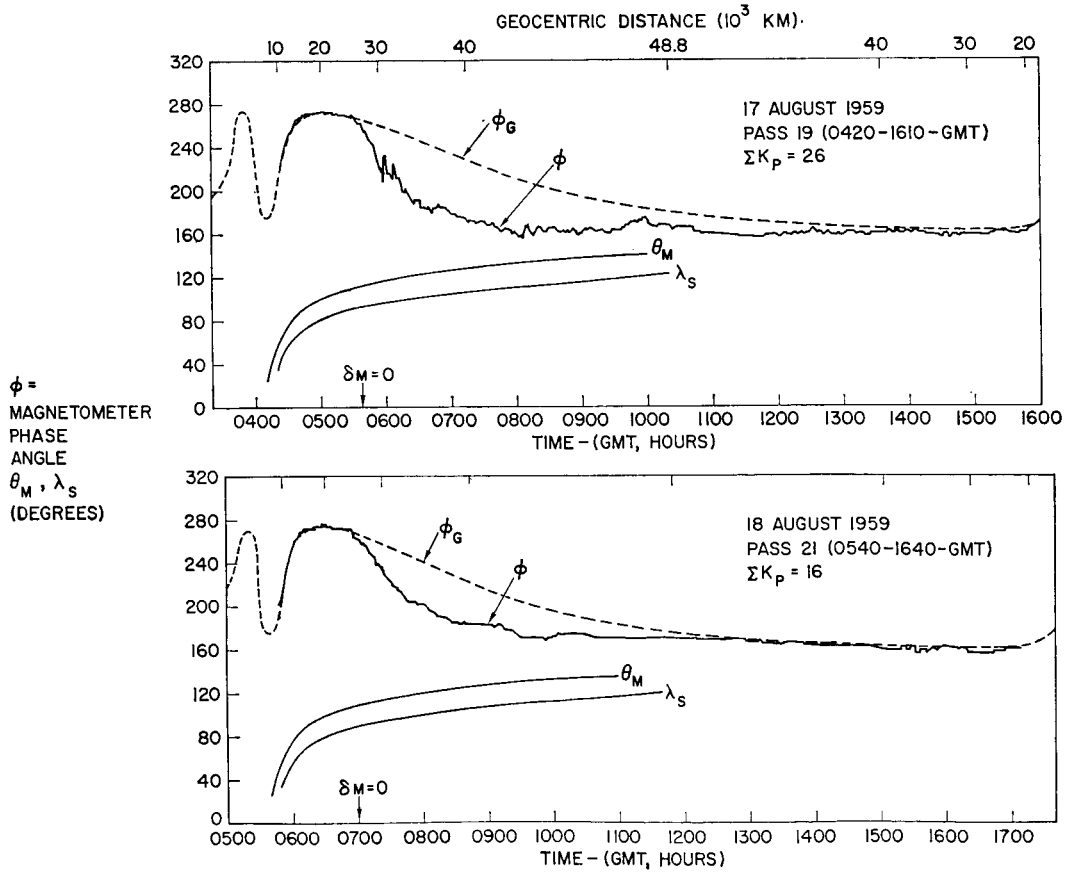

Fig. 9. Phase data obtained during a magnetic storm (odd-numbered passes). The empirical phase angle and the theoretical angles presented in Figure 8 are shown here for passes 19 and 21 on August 17 and 18.

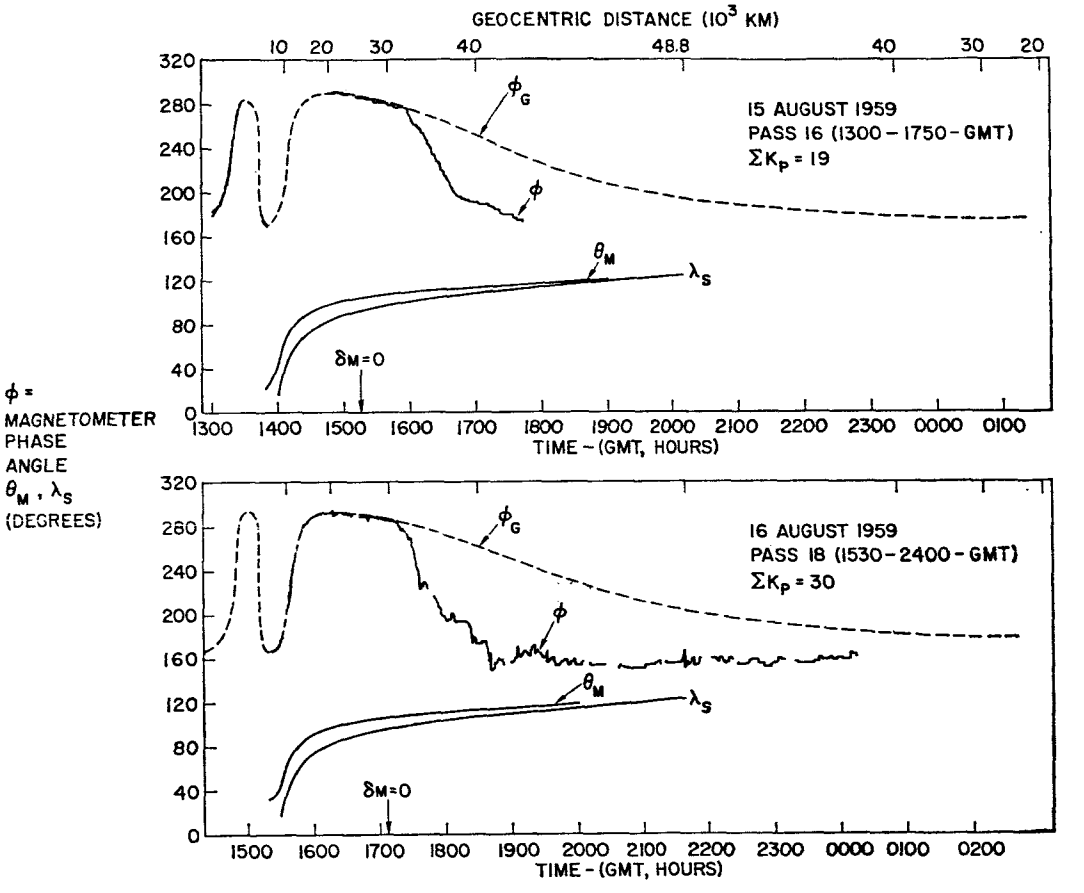

Fig. 10. Phase data obtained during a magnetic storm (even-numbered passes). The phase data and theoretical angles are presented for the two even-numbered passes on August 15 and 16.

These observations are qualitatively consistent with a decreased westward current in the magnetosphere.

Another feature of Figure 7 is the occurrence of fine structure during the magnetic storms. Several distinct transients (such as those seen at 30,000 km on August 17 and at 42,000 km on September 4) correlated with pulsating magnetic bays in the Antarctic [*Smith and Judge*, 1961] and transient increases in the Explorer 6 scintillator count rate. According to *Rosen and Farley* [1961], the occurrence of rapid variations in the scintillator count rate was typical of magnetically disturbed periods.

Figures 8 through 11 contain the phase angle data for eight successive orbital passes during August 15–18. $\sum K_p$ is the sum of the 3-hour planetary K indices during the 12-hour period corresponding to each orbital pass of Explorer 6. The altitude at which the spacecraft crossed the geomagnetic equatorial plane is denoted in each figure by $\delta_M = 0$ and an arrow (see Figure 14 for the position of the spacecraft at other geomagnetic latitudes). θ_M is an angle between $\hat{\omega}$, the Explorer 6 spin axis, and n, the normal to the local magnetic meridian plane (Figure 12). The meridian plane contains the local field direction and the center of the earth. The perpendicular to the magnetic meridian plane is given by $\hat{e}_B \times \hat{e}_R$, where $\hat{e}_B$ is a unit vector in the direction of the extrapolated geomagnetic field, and $\hat{e}_R$ is a unit vector in the direction from the earth's center to the spacecraft. The extent to which the spacecraft spin axis was rotated out of the magnetic meridian plane at different points along the trajectory is indicated

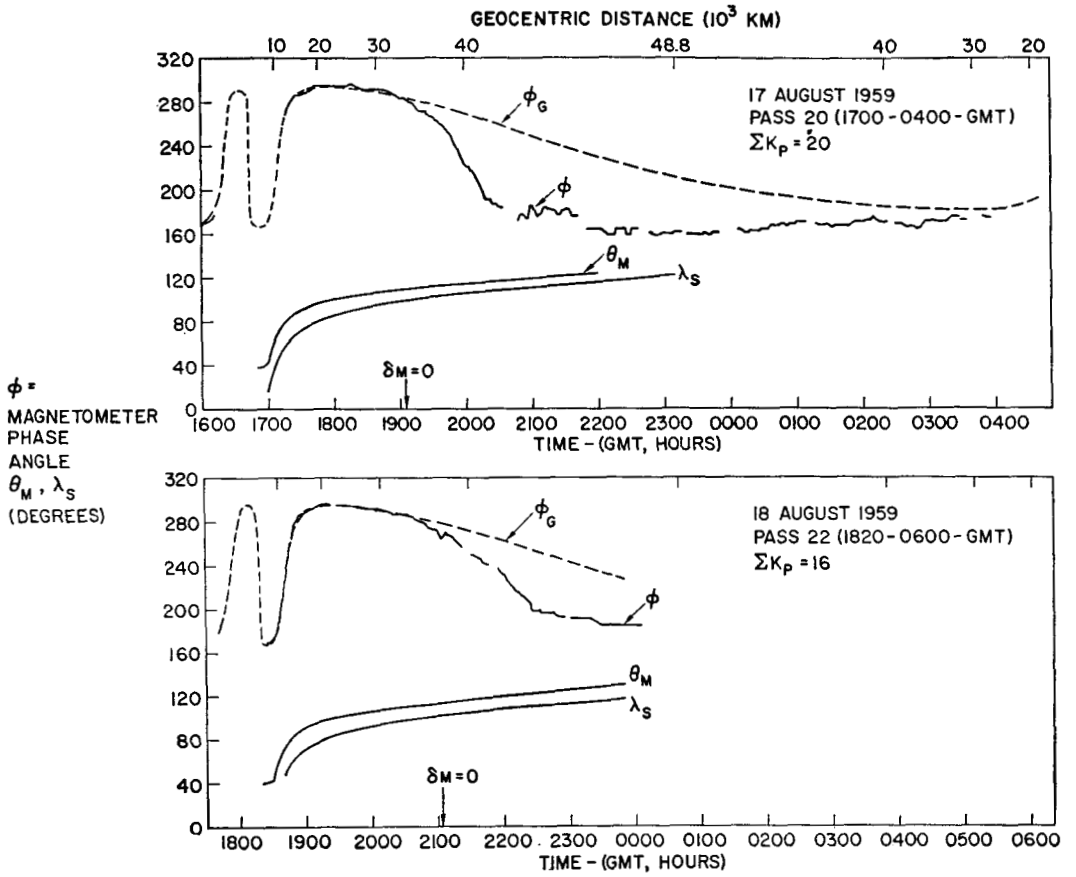

Fig. 11. Phase data obtained during a magnetic storm (even-numbered passes). The phase data and theoretical angles are presented for two even-numbered passes on August 17 and 18.

by θ_M. The angle λ_s is obtained when the earth-sun vector and the satellite radius vector are projected onto the equatorial plane (Figure 13).

As discussed earlier, the data are divided into two groups in order to minimize trajectory effects. Figures 8 and 9 contain only the odd-numbered passes which generally occurred during the first half of the Greenwich day, whereas Figures 10 and 11 contain even-numbered passes. There were small progressive changes in the geomagnetic coordinates of the spacecraft at a given point on the trajectory on the odd-numbered and even-numbered orbits taken alone. In Figures 14 and 15 the altitude at which δ_M was zero progressed to higher altitudes during the odd-numbered passes and to lower altitudes during the even-numbered passes.

Figures 8 through 11 show a progressive enhancement of $\Delta\varphi$ during the storm with a subsequent return to prestorm values. This can be seen if we consider a given $\Delta\varphi$ (e.g., $\Delta\varphi = -20°$), which moved toward lower altitudes during the main phase of the storm ($\sum K_p$ increasing) and returned to higher altitudes during the recovery phase ($\sum K_p$ decreasing).

Figure 16 provides an alternative view of the variations in $\Delta\varphi$ during the storm. At the top of the figure is a plot of $\Delta\varphi$ at a given altitude (40,000 km) as a function of time. The simultaneous variation in the horizontal intensity at the earth's surface is plotted in the middle of the figure. The data are hourly mean values of H at Huancayo. The diurnal variation has been removed. At the bottom of the figure is a plot of the corresponding values of the 3-hour index K_p. The direction of the distant field was corre-

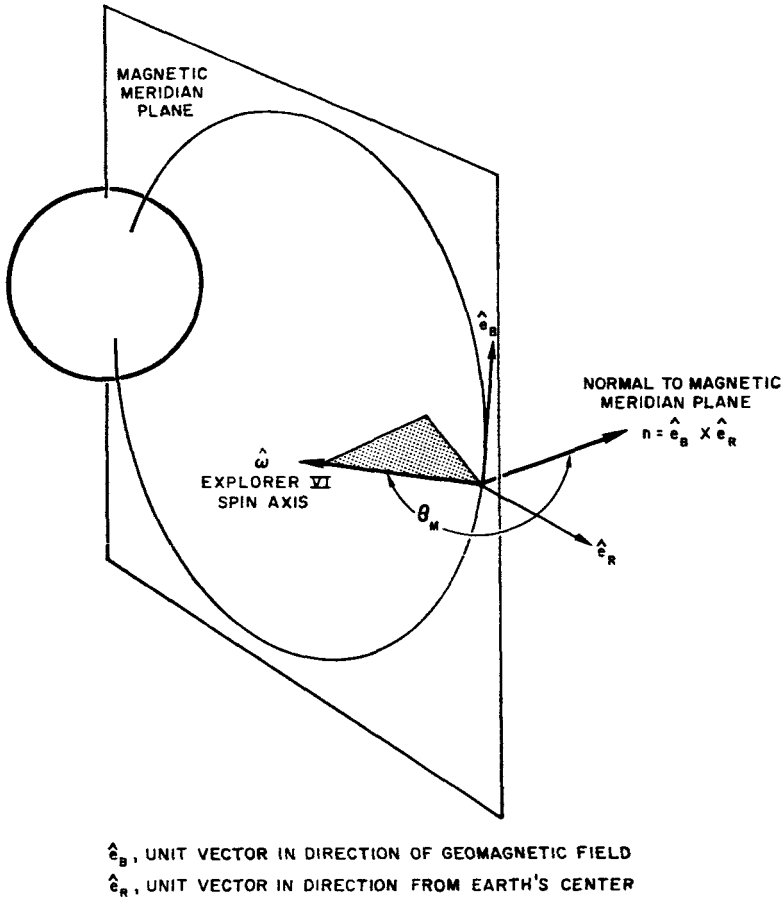

Fig. 12. Representation of the angle θ_M. The unit vector $\hat{e}_B$ gives the direction of the geomagnetic field. $\hat{e}_R$ is a unit vector parallel to the radius vector from the center of the earth to the instantaneous position of the spacecraft. $\hat{n}$ is the unit normal to the local magnetic meridian plane, i.e., the plane of the geomagnetic field line. θ_M, the angle between the normal to the magnetic meridian plane and $\hat{\omega}$, the spacecraft spin axis, is useful in determining how sensitive the magnetometer is to disturbance field components lying in, or perpendicular to, the magnetic meridian plane.

lated with both variations in the horizontal component and the degree of agitation of the surface field.

This correlation appears to include the initial phase of the August 16 storm. However, the increase in ΔH and decrease in $\Delta\varphi$ observed during the first quarter of August 16 actually represented a superposition of two effects, the initial phase of the sudden commencement storm of August 16 and the recovery phase of the gradual commencement storm of August 15. The effect of the GC storm on the distant field can be seen in the first two data in Figure 10 (August 15) and by comparing Figures 8 (top) and 10 (top) (successive passes). An inspection of ground station magnetograms shows that the GC storm was of short duration. Because the two storms overlap, it was not possible to isolate and study the effects of the initial phase of the SC storm. The subsequent data show the effect of the main phase decrease and recovery associated with the August 16 storm.

Simultaneous variations in field magnitude and peak intensity of the outer radiation zone. Figure 17*d* is the same as Figure 6*a*, that is $\Delta B_\perp$ at $\sim 4R_E$. Measurements of the peak intensity of the radiation particle fluxes in the outer zone are also shown. Figures 17*a*, *b*, and *c* are the

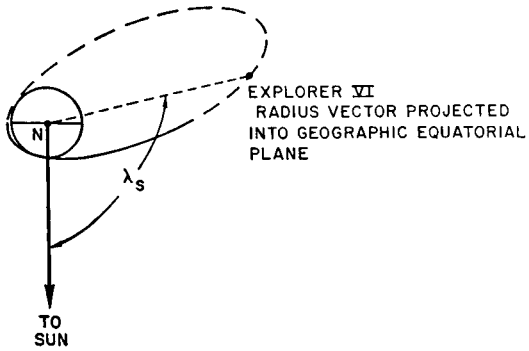

Fig. 13. Representation of the angle, λ_s. The sun-earth direction and the Explorer 6 radius vector are shown when projected on the geographic equatorial plane. λ_s, the angle between these projections, gives the instantaneous position of the spacecraft with respect to the sun-earth direction. The projected Explorer 6 orbit for August 16 was used as an example. The solid part of the orbit lies above, and the dashed part below, the equatorial plane.

Explorer 6 data obtained by the Space Technology Laboratories scintillation counter, the University of Chicago proportional counter, and the University of Minnesota Geiger tube. Before the storm of August 16, the primary peak in the outer zone was at approximately 24,000 km, on the basis of Geiger tube data [*Arnoldy et al.*, 1960]. Thus, equatorial field measurements and Geiger tube measurements of the peak intensity occur in the same region of space and are essentially simultaneous. The peak of the outer zone as detected by the other two instruments was displaced slightly from 24,000 km [*Fan et al.*, 1960; *Rosen and Farley*, 1961].

During the main phase of the storm, there was a substantial decrease in the count rates of the University of Minnesota and University of Chicago experiments, followed by a large increase in the particle fluxes during the recovery phase of the storm. The scintillator data departed from this general tendency only during the onset of

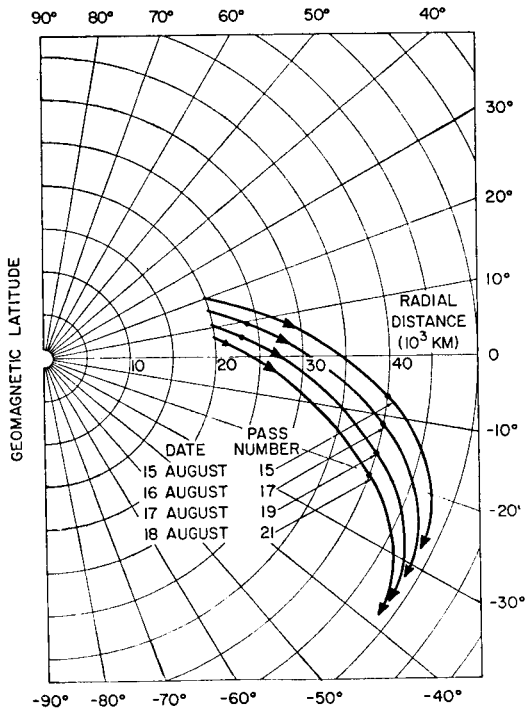

Fig. 14. Geomagnetic latitude of the spacecraft (odd-numbered passes). The part of the Explorer 6 orbit between radii of 20,000 and 48,000 km is shown for passes 15, 17, 19, and 21 on August 15–18. The triangle (digital data) and circles (analog data) mark the positions at which data used in Figures 6 and 16 were obtained.

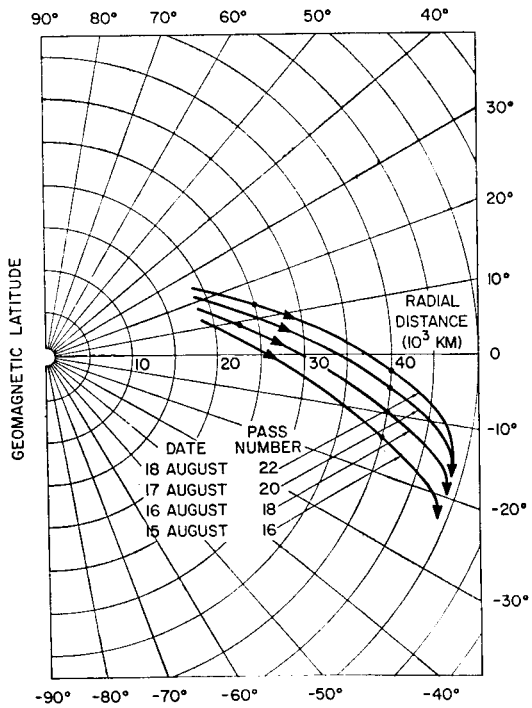

Fig. 15. Geomagnetic latitude of the spacecraft (even-numbered passes). This figure contains the trajectory in spherical coordinates (geomagnetic latitude and radial distance) for passes 16, 18, 20, and 22 on August 15–18. The circles mark the location of Explorer 6 at which the data used in Figures 6 and 16 were obtained.

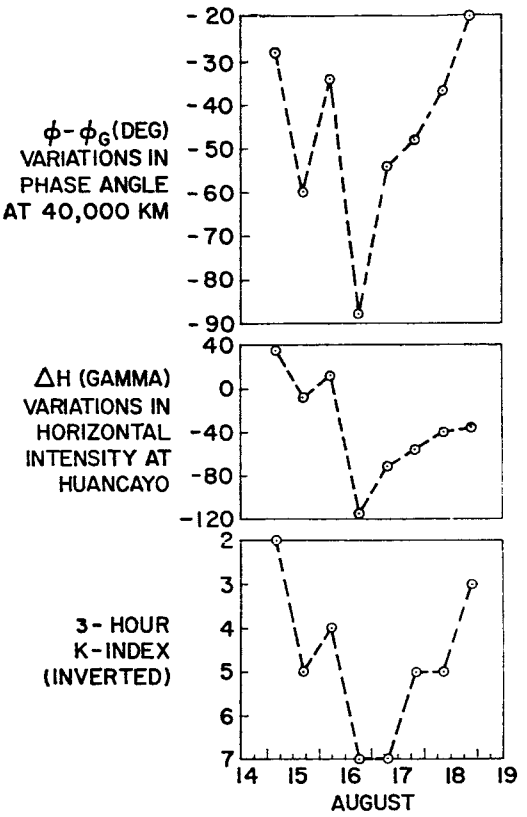

Fig. 16. Temporal variation in the phase data at 40,000 km compared with the surface field. $\phi - \phi_G$ is the phase angle deviation, observed minus theoretical (corresponding to the unperturbed geomagnetic field). $\phi - \phi_G$ is shown during the storm interval August 15–18. Each Explorer 6 datum was obtained at a geocentric altitude of 40,000 km irrespective of geomagnetic latitude (see Figures 14 and 15). ΔH shows the variation in the average value of the horizontal component at Huancayo for the hour during which the Explorer 6 data were obtained. The three-hour K index, inverted so that K increases downward, is shown in the lower third of the figure. Note the correspondence between variations in the surface field and in the field direction at $\sim 6.3 R_E$ (40,000 km). Two storms are superposed. A gradual commencement storm that began August 15 was in the recovery phase when a sudden commencement storm began on August 16.

the main phase. This behavior is characteristic of the outer zone during a magnetic storm and has been observed by similar instruments on other satellites. The responses of the Explorer 6 detectors are consistent with the subsequent empirical demonstration that, with the onset of a magnetic storm, the low-energy (100 kev or less) particle flux increases at the same time that the medium- and high-energy particle fluxes are decreasing. All three components then undergo a large increase during the recovery phase of the storm [e.g., *Obrien*, 1964].

Figure 17 shows that the slow variations in particle intensity were correlated with the variations in field magnitude at $4R_E$. However, although the peak intensities in the outer zone after the storm increased by an order of magnitude, the magnetic field intensity was still somewhat less than it's prestorm value.

Summary

The experimental data can be summarized as follows:

1. Long-period time-dependent changes in the distant field coincided with D_{st} at the surface.
2. The magnitude of the main phase decrease in $B_\perp$ was ~ 2.5 times larger at $\sim 4R_E$ than at the surface.
3. Irregular field fluctuations, with periods exceeding one minute, were observed during the storm.
4. Variations in the direction of the field at $\sim 7R_E$ correlate with half-day variations in (*a*) the horizontal component of the surface field and (*b*) the three-hour planetary K index.
5. The large-scale perturbations of $B_\perp$ and φ during the storm were qualitatively similar to the perturbations observed previously on nonstorm days.
6. The D_{st} variations in the field magnitude at $4R_E$ correlate with changes in the peak intensity of the outer radiation zone measured by three high-energy particle detectors on Explorer 6. Two detectors show a decreased intensity during the storm when the field magnitude is depressed. All three detectors recorded peak intensities that exceeded the prestorm values by an order of magnitude at the same time that the field magnitude returned to its quiescent value.

Discussion

Characteristics of the large-scale storm field. The storm data at 4 to $8R_E$ and the worldwide component of the surface storm field (D_{st}) have the same time dependence. Furthermore, the variations at 1, 4, and 7 earth radii are essentially

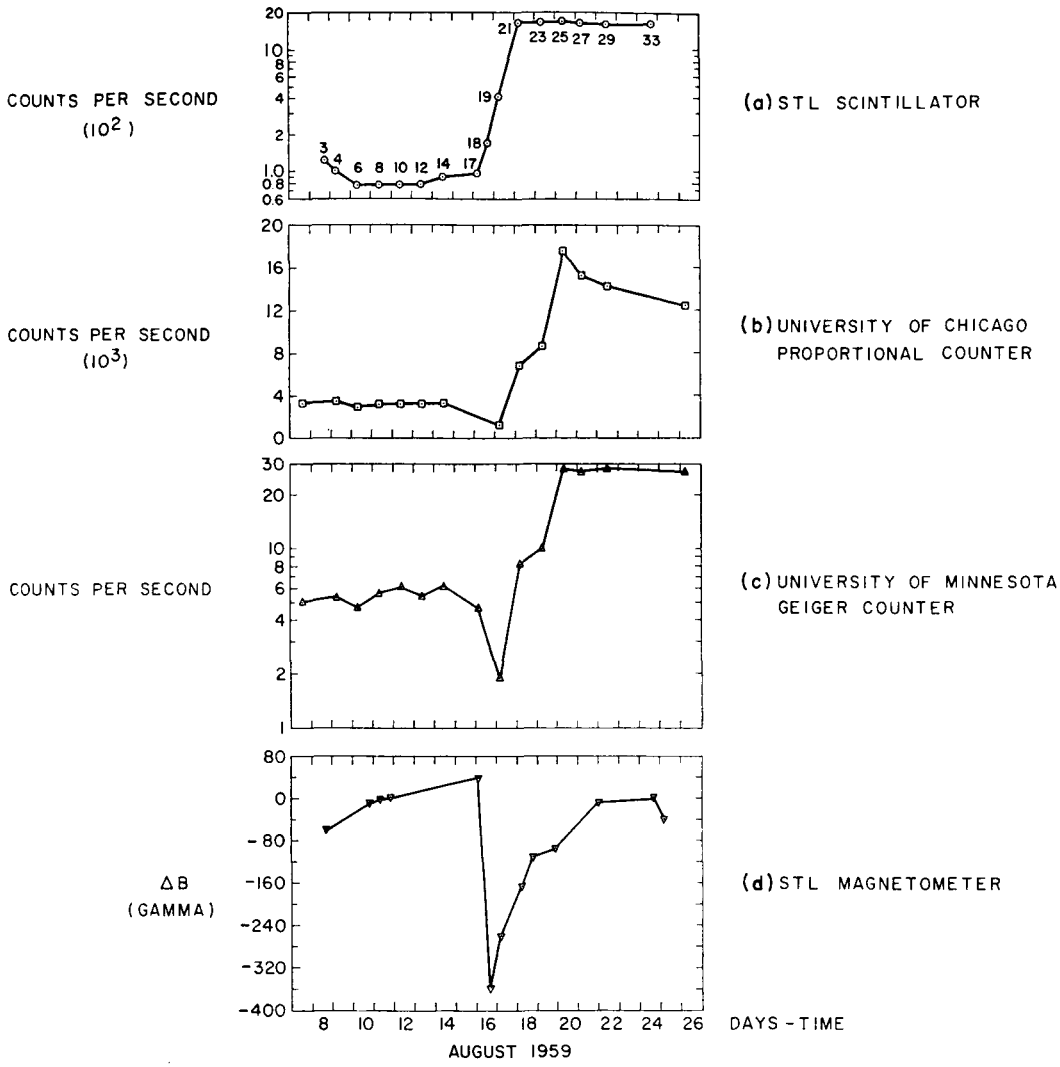

Fig. 17. Comparison of equatorial magnetic field variation at $4R_E$ with simultaneous variation in the three Explorer 6 particle detectors. The time dependence of the peak counting rate per orbit of the scintillating crystal detector (STL) appears at the top. The variation in the coincidence telescope (University of Chicago) peak counting rate is shown as the next lower curve. The maximum count rate per orbit obtained by the Geiger counter (University of Minnesota) as a function of time is given by the next lower curve. The magnetometer data that appear at the bottom of the figure are the same data that appear in Figure 6.

simultaneous, that is, possible time delays are much less than the characteristic period of the D_{st} variation. During the storm, the earth was immersed in a large-scale magnetic field that was manifest at the surface as the main phase decrease.

The characteristics of the D_{st} field at the earth's surface can be described simply. The field is approximately uniform and antiparallel to the earth's axis of rotation over the entire surface.

Ideally, a complete description is desired of the magnitude and direction of the D_{st} field in the space surrounding the earth. However, a complete description is not possible from a single orbiting satellite. It is particularly difficult to distinguish between a radial dependence and a dependence on latitude or longitude when the

trajectory is a highly inclined ellipse such as the Explorer 6 orbit. In addition, useful data from Explorer 6 are restricted to parts of the orbit where the magnitude of the disturbance field was at least several per cent of the magnitude of the unperturbed geomagnetic field, as discussed previously. We can, however, infer several important properties of the large-scale storm field from the Explorer 6 data. Later magnetometer experiments can extend and improve this description.

We now show that near the equatorial plane at $4R_E$ the storm field (ΔB as distinct from $\Delta B_\perp$) was directed southward, was aligned with the local magnetic meridian plane, and had a magnitude of $\sim$350 γ. At 24,000 km, the angle θ_M between the spacecraft spin axis and the normal to the local magnetic meridian plane was approximately 105°. Thus, the spin axis was nearly contained in the meridian plane. Consequently, field rotations out of, or transverse to, magnetic meridian planes were readily detectable, while along this part of the orbit the phase angle was insensitive to rotations confined to magnetic meridian planes, which would leave φ equal to φ_G. The phase data (Figures 8 through 11) show that $\Delta\varphi$ did not exceed 8° during the storm. Therefore, any component of field rotation out of the magnetic meridian plane was small. The 350 γ decrease in $B_\perp$ during the main phase is consistent with a reduction in the magnitude of the field component parallel to G by a factor of approximately 2. Assuming that the field rotated without a change in magnitude implies a rotation of 60° which would produce a field with a large radial component near the equator. Such a field would differ greatly from the geomagnetic field and would correspond, for example, to an interplanetary field or a strongly deformed magnetic tail existing at 24,000 km and lying in a magnetic meridian plane. The experimental evidence discussed above, including the Explorer 6 trapped particle measurements, makes it certain that Explorer 6 was inside the geomagnetic field, particularly at 24,000 km. Therefore, it seems reasonable to conclude that the decrease in $B_\perp$ is primarily a decrease in magnitude, that B and G were parallel near the equator, and that $\Delta B(t)$ *in Figure 6 is approximately the magnitude of the time-varying storm field near the geomagnetic equatorial plane.* Small deviations in field direction cannot be ruled out but are not an essential feature in view of the arguments presented here.

Ring current. The disturbance observed during the storm is very suggestive of a ring current. To understand why the evidence is inconclusive, it is instructive to consider what observations would be needed for rigorous detection of this current. To deduce the current from measurements of the magnetic field, it is necessary to obtain $\oint \mathbf{B}\cdot d\mathbf{S}$ round a closed curve, thus giving the current through that closed curve. Not only does Explorer 6 lack one component of **B**, but no single satellite moves in a closed curve that is really suitable for this purpose. One possibility might be to use two satellites whose orbits are nearly coplanar and to compute the current through the lines between their orbits. In any event, quite accurate magnetic measurements would be needed. Here, then, we must be content to compare the observed field with that predicted for a ring current.

The ring current predicted is caused by trapped particles and can be regarded as arising either from their anisotropic pressure distorting the field hydromagnetically or from a combination of their drifts and diamagnetic effect. The latter is similar to pressure and causes an important depression of the field strength where the pressure is high, roughly according to pressure balance between particles and field. *Davis and Williamson* [1963] have observed a population of trapped protons having a pressure substantially higher than that of other known trapped particles. For $L > 4$ they found the pressure to be about one-tenth that of the magnetic pressure during quiet times, and they found that pressure increased by a factor of 3 during one storm. *Akasofu* [1963] has reviewed ring current theory and estimated the effect of the protons observed by Davis and Williamson. Whereas the disturbance at the ground corresponds to a westward current, the current due to trapped particles is eastward on the inner side of the particle distribution where the particle pressure is increasing with L. The westward current flows on the outer side, and the resulting disturbance is illustrated by Akasofu's computations. He obtains for storm conditions in the equatorial plane a depression of 100 γ at the ground, a maximum depression of somewhat more than 200 γ between $L = 3$ and 4, and a slight strengthening of the field beyond $L = 6$. The greater depression at $L = 4$ than at the ground is in qualitative agreement with data

from Explorer 6 and is due to the eastward current close in. The lack of detailed agreement could arise as follows. First, only protons of >100 kev were observed by Davis and Williamson, and softer protons might be important. Since the observed proton pressure went up to one-third of the magnetic pressure, the pressure of softer particles could hardly be a dominant proportion, but it could change the maximum field depression from 220 γ to, say, 350 γ. Second, the storm observed by Explorer 12 was of course not the same as that observed by Explorer 6, and substantial differences between different storms seem to be allowable. Third, Akasofu's calculation is not self-consistent. Finally, should the ring current be incapable of accounting fully for the observed disturbance on the trajectory of Explorer 6, the field farther out is known to be distorted in a quite different way. This distortion is not symmetric about the geomagnetic axis, but, for the late evening meridian of Explorer 6, there is some similarity with the changes of φ observed near apogee; this distortion will now be discussed briefly.

Distortion of the field in the outer magnetosphere. The solar wind, now certified by Mariner [*Neugebauer and Snyder*, 1962], distorts the magnetosphere. Many theoretical studies of this distortion have been published [e.g., *Midgley and Davis*, 1963]; most have neglected any interplanetary magnetic field, though some have considered it [e.g., *Dungey*, 1963]. Observations of this distortion were obtained from Explorers 10, 12, and 14. For comparison with Explorer 6, Explorers 10 and 14 are most relevant, having apogee in the evening direction. *Heppner et al.* [1963] found a boundary far out, but for the first 15 earth radii the field strength gradually exceeded the dipole value while the direction gradually swung around and pointed away from the earth (the apogees of Explorers 6, 10, and 14 were south of the equatorial plane). *Cahill* [1964] has published the results of two successive passes of Explorer 14 near the midnight meridian that are separated by 36 hours. There was a magnetic storm two days before the first pass. On the first pass the field strength was depressed from 4 to 8 radii by a roughly constant amount, $\sim$25–50 γ; farther out the field strength remained at $\sim$50–75 γ right out to apogee at 16 radii. On the second pass, there was no depression and the field strength settled at 30–50 γ from 10 radii out to apogee. On both passes the direction swung around and settled pointing away from the earth, the swing occurring between 7 and 9 radii on the first pass and between 9 and 11 radii on the second pass. It is this change in direction observed by Explorer 10 and by Explorer 14 which resembles the change in field direction observed by Explorer 6 near apogee (Cahill also found this change of direction on passes of Explorer 14 for which data have not been published). The far field near the noon meridian was observed by Explorer 12 [*Cahill and Amazeen*, 1963] and behaves entirely differently, demonstrating that the distortion is quite asymmetric and therefore not due to a ring current alone.

The observations seem to fit Dungey's model, though further measurements are required to fill in the picture. The outstanding features in this theoretical model are two concentrated current sheets, in both of which the current flows in the direction opposite to the orbital motion of the earth, the return current not being concentrated in sheets. One sheet is on the day side, is oriented normal to the direction of the sun, contains current flowing eastward, and has been found by Explorer 12. The other is on the night side, oriented roughly in the equatorial plane, contains current flowing westward, and has not yet been found. The existence of the latter current sheet is, however, consistent with the observations far out and south of the equatorial plane. Because the sheet current is westward, the effect at 6 radii is hard to distinguish from the effect of a ring current, and the nature of the distinction needs consideration.

Distinction between the ring current and distortion by the solar wind. It has been stated that the ring current can be derived from the balance between the anisotropic pressure of the trapped particles and the force density $j \times B/c$. The distortion by the wind is derived by consideration of the plasma flow resulting from the imbalance between these same forces, but only a qualitative theoretical picture has yet been obtained. However, this shows that the two effects cannot be distinguished rigorously in terms of physical mechanisms, and this is true a fortiori if the trapped particles originate from the solar wind, as seems likely because of their storm-time variation. The distinction can then only be geometrical. The axial symmetry of the ring

current contrasts with the asymmetry of the observed field far out, and it is clear that the relative importance of the wind distortion increases with the distance from the earth. Both disturbances are established beyond reasonable doubt, but it will never be easy to rigorously separate the two.

Acknowledgments. We want to express our appreciation to our colleagues, P. J. Coleman, Jr., who was involved in the initial effort to reduce the phase data, K. Moe for his careful refinement of the Explorer 6 trajectory, Professor J. A. Simpson and Professor J. Winckler for making ground station and satellite data available to us, and Dr. A. J. Dessler and Dr. R. C. Wentworth for many helpful discussions regarding ring current theory.

We are grateful to Space Technology Laboratories, Inc., and particularly to Dr. Rosen and the Space Physics Department for their cooperation and assistance in the performance of this task. Technical assistance was provided by J. Kinsey, N. Lyke, and G. Komatsu of the Space Physics Department and by I. Kliger and P. Lipinski of the Computation and Data Reduction Center.

This work was supported financially by the National Aeronautics and Space Administration under contract NASw-270.

References

Akasofu, S.-I., Deformation of magnetic shells during magnetic storms, *J. Geophys. Res., 68,* 4437–4445, 1963.

Akasofu, S.-I., J. Cain, and S. Chapman, The magnetic field of a model radiation belt, numerically computed, *J. Geophys. Res., 66,* 4013, 1961.

Akasofu, S.-I., and S. Chapman, The ring current, geomagnetic disturbance, and the Van Allen belts, *J. Geophys. Res., 66,* 1321, 1961.

Apel, J. R., S. F. Singer, and R. C. Wentworth, Effects of trapped particles on the geomagnetic field, in *Advances in Geophysics,* vol. 9, edited by H. E. Landsberg and J. Van Miegham, pp. 132–188, Academic Press, New York, 1962.

Arnoldy, R. L., R. A. Hoffman, and J. R. Winckler, Observations of the Van Allen radiation during August and September 1959, part 1, *J. Geophys. Res., 65,* 1361, 1960.

Cahill, L. J., Jr., Preliminary results of magnetic field measurements in the tail of the geomagnetic cavity, in press, 1964.

Cahill, L. J., and P. G. Amazeen, The boundary of the geomagnetic field, *J. Geophys. Res., 68,* 1835–1843, 1963.

Coleman, P. J., C. P. Sonett, D. L. Judge, and E. J. Smith, Some preliminary results of the Pioneer 5 magnetometer experiment, *J. Geophys. Res., 65,* 1856, 1960.

Davis, L. R., and J. M. Williamson, Low energy trapped protons, in *Space Research, Proc. Intern. Space Sci. Symp., 3rd, Washington, 1962,* pp. 365–375, North-Holland Publishing Company, Amsterdam, 1963.

Dungey, J. E., Null point in space plasmas, paper presented at Symp. Plasma Space Sci., Catholic University of America, June 11–14, 1963.

Fan, E. Y., P. Meyer, and J. A. Simpson, Trapped and cosmic radiation measurements from Explorer 6, in *Space Research, Proc. Intern. Space Sci. Symp., 1st, Nice, 1960,* edited by H. Kallmann-Bijl, p. 951, North-Holland Publishing Company, Amsterdam, 1960.

Heppner, J. P., N. F. Ness, C. S. Scearce, and T. L. Skillman, Explorer 10 magnetic field measurements, *J. Geophys. Res., 68,* 1–46, 1963.

Heppner, J. P., J. D. Stolarik, I. R. Shapiro, and J. C. Cain, Project Vanguard magnetic field instrumentation and measurements, in *Space Research, Proc. Intern. Space Sci. Symp., 1st, Nice, 1960,* edited by H. Kallmann-Bijl, p. 982, North-Holland Publishing Company, Amsterdam, 1960.

Judge, D. L., A. R. Sims, and M. G. McLeod, The Pioneer 1, Explorer 6, and Pioneer 5 high sensitivity transistorized search coil magnetometer, *IRE Trans. Space Electron. Telemetry, 6,* 114, 1960.

Krassovsky, V. I., Results of scientific investigations made by Soviet sputniks and cosmic rockets, *Astronaut. Acta, 6,* 32, 1960.

Lincoln, J. V., Geomagnetic and solar data, *J. Geophys. Res., 65,* 788, 1960.

Midgley, J. E., and L. Davis, Jr., Calculation by a moment technique of the perturbation of the geomagnetic field by the solar wind, *J. Geophys. Res., 68,* 5111–5123, 1963.

Neugebauer, M., and C. W. Snyder, The solar plasma experiment (in Mariner 2), *Science, 138,* 1095–1097, 1962.

Obrien, B. J., High latitude geophysical studies, with satellite Injun 3, part 3, *J. Geophys. Res., 69,* 13, 1964.

Rosen, A., and T. A. Farley, Characteristics of the Van Allen radiation zones as measured by the scintillation counter on Explorer 6, *J. Geophys. Res., 66,* 2013–2028, 1961.

Smith, E. J., A comparison of Explorer 6 and Explorer 10 magnetometer data, *J. Geophys. Res., 67,* 2095, 1962.

Smith, E. J., P. J. Coleman, D. L. Judge, and C. P. Sonett, Characteristics of the extraterrestrial current system: Explorer 6 and Pioneer 5, *J. Geophys. Res., 65,* 1858, 1960.

Smith, E. J., and D. L. Judge, Transient variations in the extraterrestrial magnetic field (abstract), *J. Geophys. Res., 66,* 2562, 1961.

Smith, E. J., and C. P. Sonett, Satellite observations of the distant field during magnetic storms: Explorer 6, *Proc. Intern. Conf. Cosmic Rays Earth Storm, Kyoto, Sept. 1961, J. Phys. Soc. Japan, 17,* 17, 1962.

Sonett, C. P., D. L. Judge, and J. M. Kelso, Evidence concerning instabilities in the distant geomagnetic field: Pioneer 1, *J. Geophys. Res., 64,* 941, 1959.

Sonett, C. P., D. L. Judge, A. R. Sims, and J. M. Kelso, A radial rocket survey of the distant geomagnetic field, *J. Geophys. Res., 65,* 55, 1960.

Sonett, C. P., E. J. Smith, D. L. Judge, and P. J. Coleman, Current systems in the vestigial geomagnetic field: Explorer 6, *Phys. Rev. Letters, 4,* 161, 1960.

Sonett, C. P., E. J. Smith, and A. R. Sims, Surveys of the distant geomagnetic field: Pioneer 1 and Explorer 6, in *Space Research, Proc. Intern. Space Sci. Symp., 1st, Nice, 1960,* edited by H. Kallmann-Bijl, p. 921, North-Holland Publishing Company, Amsterdam, 1960.

Vestine, E. H., Lines of force of the geomagnetic field in space, *Planetary Space Sci., 1,* 285, 1959.

(Manuscript received January 30, 1964; revised March 18, 1964.)